Bulk superconductivity at 38 K in a molecular system

ALEXEY Y. GANIN[1]*, YASUHIRO TAKABAYASHI[2]*, YAROSLAV Z. KHIMYAK[1], SERENA MARGADONNA[3], ANNA TAMAI[3], MATTHEW J. ROSSEINSKY[1†] AND KOSMAS PRASSIDES[2†]

[1]Department of Chemistry, University of Liverpool, Liverpool L69 7ZD, UK
[2]Department of Chemistry, University of Durham, Durham DH1 3LE, UK
[3]School of Chemistry, University of Edinburgh, Edinburgh EH9 3JJ, UK
*These authors contributed equally to this work
†e-mail: M.J.Rosseinsky@liverpool.ac.uk; K.Prassides@durham.ac.uk

Published online: XX Month XXXX; doi:10.1038/nmatXXXX

C_{60}-based solids[1] are archetypal molecular superconductors with transition temperatures (T_c) as high as 33 K (refs 2–4). T_c of face-centred-cubic (f.c.c.) A_3C_{60} (A = alkali metal) increases monotonically with inter C_{60} separation, which is controlled by the A^+ cation size. As Cs^+ is the largest such ion, Cs_3C_{60} is a key material in this family. Previous studies revealing trace superconductivity in Cs_xC_{60} materials have not identified the structure or composition of the superconducting phase owing to extremely small shielding fractions and low crystallinity. Here, we show that superconducting Cs_3C_{60} can be reproducibly isolated by solvent-controlled synthesis and has the highest T_c of any molecular material at 38 K. In contrast to other A_3C_{60} materials, two distinct cubic Cs_3C_{60} structures are accessible. Although f.c.c. Cs_3C_{60} can be synthesized, the superconducting phase has the A15 structure based uniquely among fullerides on body-centred-cubic packing. Application of hydrostatic pressure controllably tunes A15 Cs_3C_{60} from insulating at ambient pressure to superconducting without crystal structure change and reveals a broad maximum in T_c at ∼7 kbar. We attribute the observed T_c maximum as a function of inter C_{60} separation—unprecedented in fullerides but reminiscent of the atom-based cuprate superconductors—to the role of strong electronic correlations near the metal–insulator transition onset.

The Cs_xC_{60} phase field is poorly understood around the critical $x = 3$ composition. Face-centred-cubic (f.c.c.) Cs_3C_{60} (Fig. 1c) has been a key target since the discovery of superconductivity in these materials, but direct synthesis by thermal combination of Cs and C_{60} in gas–solid or solid–solid reactions has been unsuccessful[5]. This is ascribed to competition from the stable Cs_1C_{60} and Cs_4C_{60} phases, driven by the size mismatch between the large Cs^+ cation and the small tetrahedral site in the f.c.c. array, which is thought to prevent the formation of f.c.c. Cs_3C_{60}. Synthesis at the Cs_3C_{60} starting composition has produced superconductivity with only ∼1% shielding fraction at ambient (Cs, CsBi and other intermetallics as Cs sources, $T_c = 30$ K) (refs 6,7) and high pressures (reduction of C_{60} with Cs dissolved in liquid ammonia, $T_c = 40$ K at 14 kbar) (ref. 8) precluding identification of the phase responsible, which has variously been assigned body-centred-cubic, tetragonal and orthorhombic symmetry[8–10]. The development of low-temperature solution-based routes to alkali metal fullerides has concentrated on the use of liquid ammonia as a solvent. Here, we use methylamine[11–13] to prepare solvated precursors with a suitable Cs distribution and structure to nucleate the bulk formation of superconducting Cs_3C_{60}.

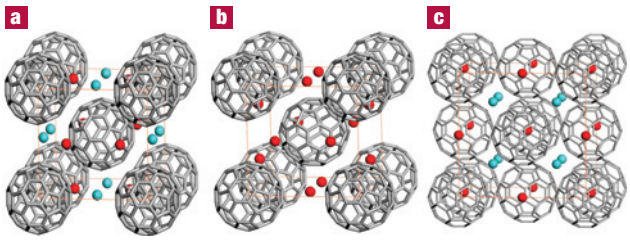

Figure 1 Candidate crystal structures for Cs_3C_{60}. **a**, b.c.o. unit cell with partial (75%) occupancy of the indicated cation sites (space group $Immm$). **b**, A15 unit cell (space group $Pm\bar{3}n$) based on b.c.c. anion packing. **c**, f.c.c. unit cell (space group $Fm\bar{3}m$). It is important to note that in **a** and **b** one unique orientation of the C_{60}^{3-} anions is present, whereas in **c** two orientations related by 90° rotation about [100] occur in a disordered manner. In the representation of **c** here, only one of these orientations is shown for clarity. The Cs^+ ions are shown as red and blue spheres to signify symmetry-inequivalent positions in the unit cell. In **c** the red and blue spheres correspond to octahedral and tetrahedral sites respectively, whereas in **a** the two sites differ in the anion faces presented to the cations. In **b**, one of two possible sets of cation sites is shown. The lower densities of the body-centred packings in **a** and **b** offer more spacious sites (with four fulleride neighbours) for the large Cs^+ cation.

Reaction of three equivalents of caesium with C_{60} in rigorously dried methylamine at −65 °C followed by removal of the solvent under dynamic vacuum at room temperature and heating at 180 °C for 48 h yields a material of composition $Cs_{3.08(10)}C_{60}$ (see Supplementary Information, Scheme S1). Diffraction shows that body-centred anion packing is dominant with 13.4(1)% of a body-centred-orthorhombic (b.c.o.) phase (Fig. 1a) and 77.7(6)% of a cubic phase with the so-called A15 structure ($a = 11.78282(8)$ Å, space group $Pm\bar{3}n$) in which the fulleride anion at the body centre is rotated by 90° about the [100] direction relative to the anion at the origin (Fig. 1b). A second cubic phase (8.9(2)% phase fraction) is observable with f.c.c. symmetry and a lattice constant

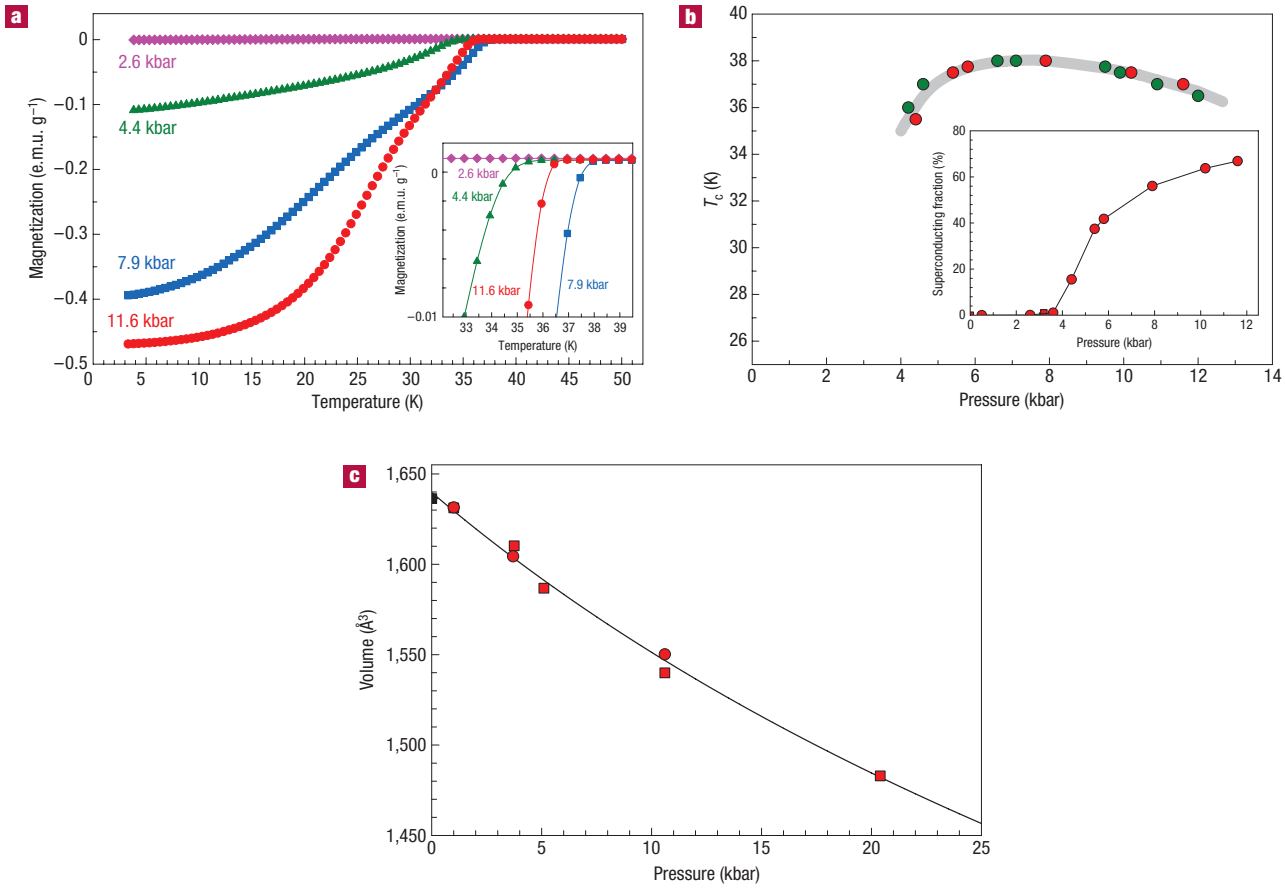

Figure 2 Superconductivity under pressure in A15 Cs_3C_{60}. **a**, Temperature dependence of the magnetization, *M* (zero-field-cooling protocol, 20 Oe), at selected pressures. The inset shows an expanded view of the data near the temperature onset of the metal-to-superconductor transition, T_c. Field-cooling and zero-field-cooling data confirming the Meissner effect are shown in Supplementary Information, Fig. S4. **b**, Evolution of T_c with change in pressure for two different A15 Cs_3C_{60} samples. T_c is defined as the temperature at which *M* begins to decrease (inset in **a**). The inset shows the pressure dependence of the superconducting fraction. Squares (circles) label data obtained with increasing (decreasing) pressure. **c**, Pressure dependence of the unit cell volume of the A15 Cs_3C_{60} phase. Squares (circles) label data obtained with increasing (decreasing) pressure. The line through the data is a guide to the eye. The volume compressibility, $\kappa = 0.054(3)$ GPa^{-1}, was extracted by a linear fit in the pressure range 0.001–10.6 kbar and is comparable to those found for Na_2CsC_{60} (0.064(4) GPa^{-1}), K_3C_{60} (0.036(3) GPa^{-1}) and Rb_3C_{60} (0.046(3) and 0.058(1) GPa^{-1}) (refs 21–23). The pressure dependence of the unit cell volume of the f.c.c. Cs_3C_{60} phase is shown in Supplementary Information, Fig. S3.

(14.802(2) Å) comparable to that predicted for Cs_3C_{60} by Vegard's law extrapolation of the $Cs_{3-x}Rb_xC_{60}$ family[14].

Low-field (20 Oe) zero-field-cooling and field-cooling d.c. magnetization, *M*, measurements reveal no superconductivity at 1 atm, but application of hydrostatic pressure (11.6 kbar) produces bulk superconductivity with a shielding fraction of 67% and an onset T_c of 37 K (Fig. 2a). The superconducting response of the sample is then followed by gradually releasing the external pressure. T_c responds sensitively, shifting initially to higher temperatures (38 K at 7.9 kbar, Fig. 2a, inset). On further depressurization, T_c first shows a plateau down to 5.8 kbar, followed by a reversal of the initial trend and a rapid decrease down to 35.5 K at 4.4 kbar (red circles, Fig. 2b). Moreover, as the pressure is gradually released below 11.6 kbar, the shielding fraction becomes progressively smaller, approaching 16% at 4.4 kbar (Fig. 2b, inset). At lower pressures (2.6–3.6 kbar), the superconducting fraction is rapidly suppressed to the level of trace superconductivity (0.1–1%) and full pressure release recovers the original non-superconducting phase. Reproducibility was confirmed by a further series of experiments (green circles, Fig. 2b) on another A15 Cs_3C_{60} sample prepared under identical conditions. Comparable measurements on b.c.o.-dominated samples without the cubic phases reveal no superconductivity at ambient or high *P*. Superconductivity can then only be attributed to either of the two cubic packings (f.c.c. and body-centred-cubic (b.c.c.)-based A15) observed in the system.

As A15 Cs_3C_{60} is the overwhelmingly dominant crystalline phase, it is logical to attribute the bulk high-T_c response to this C_{60}^{3-} compound, but to be certain we modified the synthetic procedure to generate a sample in which the large-lattice-constant f.c.c. phase was predominant over the A15 phase. f.c.c. Cs_3C_{60} has not been accessible before in the Cs_xC_{60} phase field. Reaction of reducing agent Cs_6C_{60} (rather than Cs) and C_{60} in methylamine followed by solvent removal under dynamic vacuum and heating at 100 °C (see Supplementary Information, Scheme S2) yields an analysed composition $Cs_{3.4(1)}C_{60}$, where diffraction reveals 42.0(1)% of a 14.7930(2) Å f.c.c. Cs_3C_{60} phase together with 29.0(2)% A15 and 29.0(2)% b.c.o. phases. This second sample also exhibits a pressure-induced reversible phase transition to superconductivity, but with a reduced superconducting shielding fraction (34%). Comparison of the magnetization data at 11.6 kbar (see Supplementary Information, Fig. S1) shows a much greater diamagnetic signal at the 37 K transition in the A15-dominated

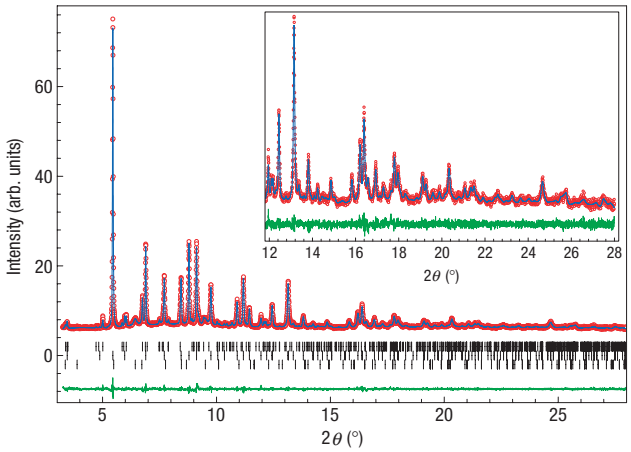

Figure 3 Structural characterization of A15 Cs_3C_{60}. Final observed (circles) and calculated (blue solid line) synchrotron X-ray ($\lambda = 0.50079$ Å) powder diffraction profile for the A15-rich sample (majority A15 phase, 77.7(6)%) at ambient temperature. The lower solid line shows the difference profile and the tick marks show the reflection positions of the A15 (top), f.c.c. (middle) and b.c.o. (bottom) phases. The inset shows an expanded view of the diffraction profile at high Bragg angles. Refined parameters and agreement indices are given in Supplementary Information, Table S2. Complementary NMR characterization described in Supplementary Information, Figs S5,S6 and Table S1 confirms the phase assemblage deduced from the diffraction data.

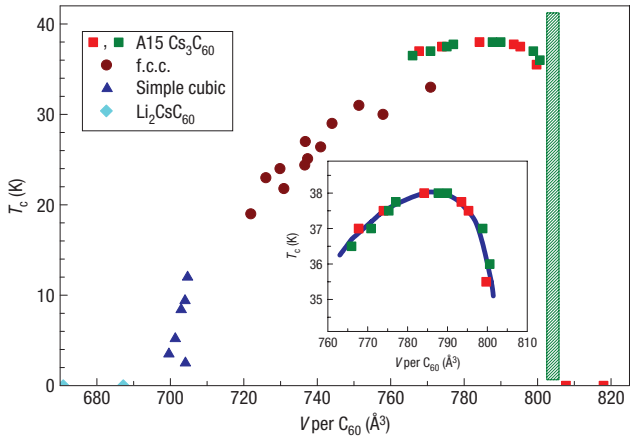

Figure 4 Superconducting transition temperature, T_c, as a function of volume occupied per fulleride anion, V, at ambient temperature. The cyan rhombi, blue triangles and brown circles correspond to f.c.c. C_{60}^{3-} anion packings with Li_2CsC_{60}, $Pa\bar{3}$ symmetry and $Fm\bar{3}m$ symmetry, respectively. The highest T_c in the $Fm\bar{3}m$ series is 33 K for Cs_2RbC_{60} (ref. 4). The red/green squares correspond to the bulk $T_c(V)$ behaviour observed in the b.c.c. anion packing of A15-structured Cs_3C_{60}. The shaded region marks the onset of the insulator–metal transition. The inset shows the maximum observed in $T_c(V)$ for A15 Cs_3C_{60}.

sample, demonstrating unambiguously that the onset T_c observed is due to the A15 Cs_3C_{60} phase.

The solvent used to access the initial precursors is key to determining the outcome of the subsequent thermal protocols to crystallize the cubic Cs_3C_{60} polymorphs. This is demonstrated by control reactions in which the synthesis of the precursors was repeated with ammonia rather than methylamine as solvent. This yields poorly crystalline materials with pronounced amorphous components—the crystalline components were dominated by the b.c.o. phase with a trace of A15 and no indication of the f.c.c. phase, and there is no significant change on heating. Once formed through the methylamine solvent route, both the A15 and f.c.c. phases are kinetically stable and do not transform into the Cs_1C_{60} and Cs_4C_{60} phases. This is the first observation of the f.c.c. Cs_3C_{60} phase, which has the largest interanion separation (10.46 Å) and volume per C_{60}^{3-} anion, V (809.3 $Å^3$), in the A_3C_{60} family, although its electronic properties are not yet clear owing to the obscuring effect of the high-T_c A15 phase in the present samples.

Superconductivity is only observed under applied pressure and therefore the phase assemblage evolution with pressure is critical to understanding its origin. We first analysed the high-resolution synchrotron X-ray diffraction data at ambient pressure (at room temperature and 10 K) to identify the structural features of the superconducting phase. The A15 structure has two possible inequivalent cation locations, each surrounded by four nearest-neighbour fulleride anions but distinguished by whether Cs^+–C_{60} closest contacts are to pentagons (Cs^+ residing in the 6*c* (1/2 1/4 0) sites of the $Pm\bar{3}n$ space group; coordination number 20) or hexagons (Cs^+ in 6*d* (1/4 1/2 0); coordination number 24) on the neighbouring C_{60}^{3-}. Rietveld refinement clearly shows (Fig. 3, Supplementary Information, Table S2) that the larger hexagon-coordinated 6*d* sites are fully occupied by Cs^+ and the 6*c* sites are empty (as shown in Fig. 1b). This more expanded of the two available coordination environments, similar to that of the tetrahedral interstices of f.c.c. A_3C_{60}, is favoured by the size of Cs^+ (mean Cs…C distance = 3.66 Å at 295 K). However, the A15 Cs_3C_{60} structure supports distinctly different C_{60}^{3-}–C_{60}^{3-} near-neighbour interactions (hexagon–hexagon facing with mean C…C interanion contacts of 3.80 Å) from those in f.c.c. A_3C_{60} (interanion contacts of 3.18 Å through neighbouring hexagon:pentagon C–C bonds in K_3C_{60}) (ref. 15). Synchrotron X-ray powder diffraction at ambient temperature with a diamond anvil cell reveals no pressure-induced structural changes in the pressure range 0.001–20.4 kbar (see Supplementary Information, Fig. S2). The Cs^+ ions remain sterically uncrowded in the tetrahedral holes with a mean Cs…C distance of 3.46 Å at 20.4 kbar, whereas the mean near-neighbour C…C contacts approach 3.47 Å. Importantly, there is also no change in the fractions of the three coexisting phases and refinement shows that the A15 phase remains dominant to the highest pressure. The extracted compressibility κ ($\equiv -d\ln V/dP$) of A15 Cs_3C_{60} is 0.054(3) GPa^{-1} (Fig. 2c), whereas that of f.c.c. Cs_3C_{60} is 0.059(4) GPa^{-1} (see Supplementary Information, Fig. S3). The phase assemblage at ambient and high pressure reinforces the conclusion that the A15 cubic Cs_3C_{60} phase is a 38 K superconductor.

The maximum superconductivity onset of 38 K at ~7 kbar in A15 Cs_3C_{60} is the highest T_c observed in a bulk molecular material. T_c of A15 Cs_3C_{60} is consistent with the monotonic $T_c(V)$ increase found in smaller-V f.c.c. fullerides (Fig. 4—V is the volume per C_{60}^{3-} anion), as the b.c.c.-based packing gives a lower anion density than all previous superconducting A_3C_{60} phases. If the electrons remained delocalized, the resulting reduction of inter C_{60} overlap would produce a narrower t_{1u} band and a higher density of states at the Fermi level, $N(E_f)$, giving an increased T_c in a simple Bardeen–Cooper–Schrieffer-like model. However, A15 Cs_3C_{60} is not superconducting at ambient pressure, unlike the f.c.c. A_3C_{60} phases. The reduction of the interanion overlap thus has a significantly greater effect than simply increasing $N(E_f)$ for itinerant t_{1u} electrons.

A narrow band or strongly correlated electronic system is defined by the competition between the onsite interelectron repulsion U (favouring localization of the electrons on their

parent atoms or molecules) and the bandwidth W (favouring delocalization), which in the simple Mott–Hubbard model produces an insulating localized electron ground state when $U > W$. Both theoretical and experimental estimates suggest that $U(\approx 1\text{–}1.5\,\text{eV}) > W(0.5\text{–}0.75\,\text{eV})$ in A_3C_{60} at all observed anion densities V (and thus all accessible bandwidths W—the U/W ratio controlling this transition can be thought of as scaling with V) (refs 3,16,17). f.c.c. A_3C_{60} has a geometrically frustrated lattice topology which, combined with the t_{1u} orbital degeneracy, generates a significantly higher critical ratio of $(U/W)_c \approx 2.3$ for electron localization, accounting for the observed metallic and superconducting behaviour[17]. The b.c.c.-based anion packing of A15 Cs_3C_{60} is not a frustrated topology, which reduces the value of $(U/W)_c$ from 2.3 to 1.3 (ref. 18), naturally placing A15 Cs_3C_{60} closer to the insulator–metal transition than the f.c.c. phases. The absence of superconductivity at ambient pressure in A15 Cs_3C_{60} can then be explained by the electron-correlation-driven localization of the t_{1u} electrons, as at the ambient pressure V of 817.9 Å^3, (U/W) exceeds the critical value. The application of pressure above ~3 kbar drives the material through the insulator–metal transition by enhancement of W through compression of the interfulleride distances—$(U/W)_c$ is reached at $V \approx 805.9$ Å^3—without the complicating effect of any crystal symmetry change, an ingredient that has been missing from all earlier studies. The absence of structural change associated with the pressure-induced insulator–metal transition in Cs_3C_{60} supports its electronic origin.

Once the superconducting state is established, T_c increases with decreasing V (Fig. 4) in complete contrast to the behaviour of the smaller-V f.c.c. K_3C_{60} and Rb_3C_{60} under pressure, reaching a broad maximum at ~7 kbar, at which point the $T_c(V)$ dependence becomes conventional, that is, controlled by the expected decrease in $N(E_f)$ as V decreases. The change in sign of $\partial T_c/\partial V$ for A15 Cs_3C_{60} is very likely associated with the tuning of its electronic structure through the exact point of the insulator–metal transition, giving a differing T_c response to decreased intermolecular separation near the insulator–metal transition than found further from it. The resulting maximum in T_c is strikingly reminiscent of the T_c (hole density) behaviour of the high-T_c copper oxides as they are chemically doped to cross the Mott–Hubbard insulator–metal transition—in the present case, however, the complicating site disorder associated with crystal-chemical substitution in the oxides is not introduced. Both the observed $T_c(V)$ phenomenology and the ability of cubic A15 Cs_3C_{60} to cross the insulator–metal phase boundary while the triple degeneracy of the t_{1u} levels is retained without any accompanying anion orientational or cation site substitutional disorder are at present unique experimental features among fulleride phases and place stringent constraints on theories of superconductivity in C_{60}^{3-} fullerides. Although a fully developed theory of C_{60}^{3-} superconductivity is currently lacking, we note that theoretical models of C_{60}^{2-} systems in which strong electronic correlations and Jahn–Teller electron–phonon coupling[19] produce local electron pairing show a maximum in $T_c(U/W)$ close to the insulator–metal transition[20]. The new synthetic chemistry that has led here to both the currently highest T_c molecular superconductor and the supposedly non-existent f.c.c. Cs_3C_{60} phase is sufficiently flexible to open the way for the isolation of new families of high-symmetry hyperexpanded fullerides required for the exploration of the electronic states at previously inaccessible intermolecular separations.

METHODS

Cs_3C_{60} samples were prepared by reaction of Cs metal or Cs_6C_{60} with C_{60} in methylamine (rigorously dried by condensation onto potassium at −78 °C and subsequent distillation after 30 min) at −65 °C using a dual-manifold high vacuum line. The sample was then warmed to room temperature followed by stirring for 1 h and solvent removal under vacuum. Subsequent thermal treatments and characterization are detailed in the Supplementary Information. Note: methylamine is volatile and flammable and should only be handled in a well-exhausted fume hood taking all appropriate precautions.

Solid-state NMR spectra were measured using a Bruker Avance DSX 400 solid-state NMR spectrometer operating at 400.13 MHz for ^{1}H and 100.13 MHz for ^{13}C. Zirconia rotors 2.5 mm in diameter were used for the measurements and the magic-angle spinning (MAS) rate was 20.0 kHz. The samples were loaded in a He-filled glove box. The ^{13}C MAS NMR spectra were acquired using ^{13}C $\pi/2$ pulses of 3.4 µs with 20.0 s repetition time. The ^{1}H MAS NMR spectra were measured using ^{1}H $\pi/2$ pulses of 2.8 µs and repetition times of 20 s. The ^{1}H and ^{13}C chemical shifts were referenced to TMS. A Stoe Stadi-P diffractometer (Cu-Kα_1 radiation, linear position sensitive detector) operating in Debye–Scherer geometry was used for phase analysis of samples sealed in 0.5-mm-diameter glass capillaries. Raman spectra were recorded on a JY LabRam-HR spectrometer operated in backscattered geometry by using 514.5 and 632.8 nm radiation and a sample area of 500 µm diameter by typical acquisition of 20 × 10 s. The calibration was carried out by referencing the spectrometer to the 520.07 cm^{-1} line of silicon. Single-phase C_{60} and Cs_6C_{60} samples were used as standards to ensure proper instrument calibration. C_{60} revealed only a weak signal at about 1,464–1,466 cm^{-1}, when the 638.2 nm laser was used; in the case of the 514.5 nm laser, a strong singlet peak at 1,464 cm^{-1} was observed. Cs_6C_{60} has a strong signal at 1,430 cm^{-1} when using both 514.5 and 633 nm lasers. The corresponding Raman shift per $1e^-$ transferred to C_{60} was about 5.66 cm^{-1}. Synchrotron X-ray diffraction data were collected at ambient temperature and 10 K using the high-resolution powder diffractometers on beamlines ID31 (0.85023 Å) and BM1 (0.50079 Å) at the European Synchrotron Radiation Facility, Grenoble. Characterizing data were also recorded at station 9.1 of the Daresbury Synchrotron Radiation Source (SRS) as the synthetic conditions were being optimized. High-pressure synchrotron X-ray diffraction experiments were carried out in a diamond anvil cell at the Daresbury SRS at station 9.5. The powder sample was loaded in a diamond anvil cell, which was used for high-pressure generation and was equipped with a steel gasket. The diameter of the diamond culet was 800 µm and the sample was introduced in a hole made in the gasket 250 µm deep and 200 µm in diameter. Silicone oil loaded in the diamond anvil cell was used as a pressure medium. Pressure was increased at room temperature and was measured with the ruby fluorescence method. The diffraction patterns were collected using an image plate detector ($\lambda = 0.44397$ Å) up to a pressure of 20.4 kbar. Masking of the strong Bragg reflections of the ruby chip and integration of the two-dimensional diffraction images were carried out with the FIT2D software. Data analysis of the diffraction profiles at both ambient and high P was carried out with the GSAS suite of Rietveld programs.

Magnetization measurements were carried out at 20 Oe on about 15 mg samples in the temperature range 1.8–50 K under both zero-field-cooling and field-cooling protocols with a Quantum Design superconducting quantum interference device magnetometer. Hydrostatic external pressure to 11.8 kbar was applied with a piston–cylinder high-pressure cell (easyLab Technologies Mcell10) using high-purity Sn as an *in situ* manometer. The error in the pressure determination is estimated to be of the order of 0.1–0.2 kbar. Daphne mineral oil was used as the pressure transmitting medium. Magnetization data were collected both on increasing and decreasing pressure conditions.

Received 29 November 2007; accepted 19 March 2008; published XX Month XXXX.

References

1. Hebard, A. F. *et al.* Superconductivity at 18 K in potassium-doped fullerene (C_{60}). *Nature* **350**, 600–601 (1991).
2. Iwasa, Y. & Takenobu, T. Superconductivity, Mott–Hubbard states, and molecular orbital order in intercalated fullerides. *J. Phys. Condens. Matter* **15**, R495–R519 (2003).
3. Gunnarsson, O. Superconductivity in fullerides. *Rev. Mod. Phys.* **69**, 575–606 (1997).
4. Tanigaki, K. *et al.* Superconductivity at 33 K in cesium rubidium fulleride ($Cs_xRb_yC_{60}$). *Nature* **352**, 222–223 (1991).
5. Zhou, O. & Cox, D. E. Structures of fullerene (C_{60}) intercalation compounds. *J. Phys. Chem. Solids* **53**, 1373–1390 (1992).
6. Kelty, S. P., Chen, C. C. & Lieber, C. M. Superconductivity at 30 K in cesium-doped fullerene. *Nature* **352**, 223–225 (1991).
7. Kinoshita, N., Tanaka, Y., Tokumoto, M. & Matsumiya, S. Superconductivity and electron spin resonance in Cs-doped C_{60}. *Solid State Commun.* **83**, 883–886 (1992).
8. Palstra, T. T. M. *et al.* Superconductivity at 40 K in cesium doped C_{60}. *Solid State Commun.* **93**, 327–330 (1995).
9. Messaoudi, A., Conard, J., Setton, R. & Beguin, F. New intercalation compounds of C_{60} with cesium. *Chem. Phys. Lett.* **202**, 506–508 (1993).
10. Fujiki, S. *et al.* Structure and Raman scattering of Cs_3C_{60} under high pressure. *Phys. Rev. B.* **62**, 5366–5369 (2000).

11. Cooke, S., Glenis, S., Chen, X., Lin, C. L. & Labes, M. New preparation of superconducting alkali-metal fullerides utilizing monomethylamine as solvent. *J. Mater. Chem.* **6**, 1–3 (1996).
12. Ganin, A. Y. *et al.* Methylaminated potassium fulleride, $(CH_3NH_2)K_3C_{60}$: Towards hyperexpanded fulleride lattices. *J. Am. Chem. Soc.* **128**, 14784–14785 (2006).
13. Takabayashi, Y., Ganin, A. Y., Rosseinsky, M. J. & Prassides, K. Direct observation of magnetic ordering in the $(CH_3NH_2)K_3C_{60}$ fulleride. *Chem. Commun.* 870–872 (2007).
14. Dahlke, P., Denning, M. S., Henry, P. F. & Rosseinsky, M. J. Superconductivity in expanded fcc C_{60}^{3-} fullerides. *J. Am. Chem. Soc.* **122**, 12352–12361 (2000).
15. Stephens, P. W. *et al.* Structure of single-phase superconducting potassium buckminsterfullerene (K_3C_{60}). *Nature* **351**, 632–634 (1991).
16. Lof, R. W., van Veenendaal, M. A., Koopmans, B., Jonkman, H. T. & Sawatzky, G. A. Band gap, excitons, and Coulomb interaction in solid fullerene C_{60}. *Phys. Rev. Lett.* **68**, 3924–2927 (1992).
17. Gunnarsson, O., Koch, E. & Martin, R. M. Mott–Hubbard insulators for systems with orbital degeneracy. *Phys. Rev. B* **56**, 1146–1152 (1997).
18. Han, J. E., Koch, E. & Gunnarsson, O. Metal–insulator transitions. Influence of lattice structure, Jahn–Teller effect, and Hund's rule coupling. *Phys. Rev. Lett.* **84**, 1276–1279 (2000).
19. Han, J. E., Gunnarsson, O. & Crespi, V. H. Strong superconductivity with local Jahn–Teller phonons in C_{60} solids. *Phys. Rev. Lett.* **90**, 167006 (2003).
20. Capone, M., Fabrizio, M., Castellani, C. & Tosatti, E. Strongly correlated superconductivity. *Science* **296**, 2364–2366 (2002).
21. Diederichs, J., Schilling, J. S., Herwig, K. W. & Yelon, W. B. Dependence of the superconducting transition temperature and lattice parameter on hydrostatic pressure for Rb_3C_{60}. *J. Phys. Chem. Solids* **58**, 123–132 (1997).
22. Zhou, O. *et al.* Compressibility of M_3C_{60} fullerene superconductors: Relation between T_c and lattice parameter. *Science* **255**, 833–835 (1992).
23. Margadonna, S. *et al.* Pressure and temperature evolution of the structure of the superconducting Na_2CsC_{60} fulleride. *J. Solid State Chem.* **145**, 471–478 (1999).

Supplementary Information accompanies this paper on www.nature.com/naturematerials.

Acknowledgements

We thank EPSRC for financial support under EP/C511794 and GR/S77820 and for access to the synchrotron X-ray facilities at the SRS (where we thank A. Lennie and M. A. Roberts for assistance on stations 9.5 and 9.1) and the European Synchrotron Radiation Facility (where we thank A. N. Fitch, W. van Beek and D. Papanikolaou for assistance on beamlines ID31 and BM1).

Author information

Correspondence and requests for materials should be addressed to M.J.R. or K.P.

Page 3

Query 1: Line no. 65

Author: 'BCS' defined as 'Bardeen–Cooper–Schrieffer'. OK?

Page 4

Query 2: Line no. 72

Author: 'MAS' defined as 'magic-angle spinning'. OK?

Query 3: Line no. 77

Author: Please provide text to define 'TMS'.

Query 4: Line no. 94

Author: 'SRS' defined as 'Synchrotron Radiation Source'. OK?

Page 5

Query 5: Line no. 34

Authors are encouraged to include a statement called 'Author Contributions' to specify the contributions of each co-author, such as experimental work, project planning, data analysis etc. The statement should be short, and refer to authors by their initials.